such a sputtering. However, we do not claim that solar wind erosion is the controlling mechanism acting on lunar rocks, which are most likely eroded by micrometeorite chipping of their surfaces (*22*).

J. P. BIBRING, J. P. DURAUD
L. DURRIEU, C. JOURET
M. MAURETTE, R. MEUNIER
Centre de Spectrométrie de Masse du Centre National de la Recherche Scientifique, 91 Orsay, France, and *Institut d'Optique Electronique du C.N.R.S., 31, Toulouse, France*

References and Notes

1. P. Eberhardt, J. Geiss, H. Graf, N. Grogler, *Geochim. Cosmochim. Acta* **2** (Suppl. 1), 1037 (1970); D. Heymann and A. Yaniv, *ibid.*, p. 1247; T. Kirsten, O. Müller, F. Steinbrunn, J. Zähringer, *ibid.*, p. 1331.
2. J. Geiss, P. Eberhardt, F. Buhler, J. Meister, P. Signer, *J. Geophys. Res.* **75**, 5972 (1970).
3. T. Gold, M. J. Campbell, B. T. O'Leary, *Geochim. Cosmochim. Acta* **3** (Suppl. 1), 2149 (1970).
4. B. W. Hapke, A. J. Cohen, W. A. Cassidy, E. N. Wells, *ibid.*, p. 2199.
5. That heavy ions (M about 200) from the solar wind should indeed produce radiation-damaged islands in silicates was first shown by W. H. Huang and R. M. Walker, *Science* **155**, 1103 (1967).
6. The electron microscope is at l'Institute d'Optique Electronique du C.N.R.S., Toulouse. The conditions of observation and methods of preparation have been described by J. Borg, L. Durrieu, C. Jouret, and M. Maurette [*Geochim. Cosmochim. Acta* **3** (Suppl. 2), 2027 (1971)].
7. H. W. Kraner, G. L. Schroeder, G. Davidson, J. W. Carpenter, *Science* **152**, 1235 (1966).
8. A. L. Turkevich, J. H. Patterson, E. J. Franzgrote, K. P. Sowinski, T. E. Economou, *ibid.* **167**, 1722 (1970); R. M. Lindstrom, J. C. Evans, R. C. Finkel, J. R. Arnold, *Earth Planet. Sci. Lett.* **11**, 254 (1971).
9. J. C. Dran, L. Durrieu, C. Jouret, M. Maurette, *Earth Planet. Sci. Lett.* **9**, 391 (1970).
10. K. Alexandre, J. Camplan, M. Ligonniere, R. Meunier, J. L. Sarrouy, H. J. Smith, B. Vassent, *Nucl. Instrum. Methods* **84**, 45 (1970).
11. P. B. Price and R. M. Walker, *J. Appl. Phys.* **33**, 3400 (1962).
12. K. B. Winterbon, P. Sigmund, J. B. Sanders, *Math. Fys. Medd.* **37**, 14 (1970).
13. P. Pellas, *Mem. Mus. Hist. Natur. Paris* **12**, 227 (1965).
14. L. Durrieu, C. Jouret, M. Maurette, paper presented at the Symposium on Physics, Chemistry and Shape of the Moon, Moscow, 1971.
15. J. Conel and D. Nash, *Geochim. Cosmochim. Acta* **3** (Suppl. 1), 2013 (1970); J. B. Adams and T. B. McCord, *ibid.* **3** (Suppl. 2), 2183 (1971).
16. See, for example, *Geochim. Cosmochim. Acta* **1** (Suppl. 2) (1971); *Fines Samples Collected by Apollo 14* (NASA TMX-58062, National Aeronautics and Space Administration, Washington, D.C., 1971).
17. J. P. Bibring, L. Durrieu, C. Jouret, O. Eugster, M. Maurette, in preparation.
18. R. L. Hines and R. Arndt, *Phys. Rev.* **119**, 623 (1960).
19. Artificial implantations with low-energy (E between 0.2 and 5 kev/amu) helium, neon, argon, krypton, and xenon ions have now been performed. They show that the thicknesses of the artificial coating, although representing a complex dynamic balance between the loss and the formation of amorphous material, roughly vary as $E^{0.5}$ and do not depend on the atomic number of the ions, when E is expressed in kev/amu. Therefore, it is possible to study the thermal properties of the ancient solar wind by analyzing the distribution of coating thicknesses in dust samples collected at various locations in the lunar regolith. A preliminary survey of such distribution, based on 130 different "counts," suggests that the energies of the solar wind ions are clustered around an average value, which is approximately constant over periods of about 100 to 1000 years. This distribution also reveals a surprisingly high frequency of periods dominated by the emission of low-energy ions (E between 0.2 and 1 kev/amu) and a steep decrease in the frequency of the high-energy periods (E greater than 1 kev/amu), when the energy of the solar wind increases.
20. E. J. Zeller and L. B. Ronca, *Icarus* **7**, 372 (1967).
21. P. H. Cadogan, G. Eglinton, J. R. Maxwell, C. T. Pillinger, *Nature* **231**, 29 (1971).
22. G. Crozaz and R. M. Walker, *Science* **171**, 1237 (1971); R. L. Fleisher, H. R. Hart, G. M. Comstock, *ibid.*, p. 1240.
23. We thank Profs. G. Dupouy and F. Perrier for their generous cooperation, Drs. R. Bernas and R. M. Walker for their very active and enthusiastic support and interest, and Dr. A. Dollfus for the use of his lunar albedo data. We also thank the National Aeronautics and Space Administration and the U.S.S.R. Academy of Sciences for lending us lunar dust samples and the Centre National de la Recherche Scientifique for funding this research.

4 October 1971; revised 26 November 1971 ■

Size Frequency Distribution of Martian Craters and Relative Age of Light and Dark Terrains

Abstract. *Light and dark terrains in and around Meridiani Sinus, mapped on the imagery from Mariner 6 and Mariner 7, were found to have significantly different cumulative size frequency distributions of craters. The light terrain on a mosaic of frames 6N11, 6N13, and 6N19 has a greater proportion of large craters and a lesser proportion of smaller craters than the dark terrain on the same frames. The light terrain is interpreted to be generally older than the dark terrain. The filling or partial filling of the smaller craters on the light terrain by surface detritus is suggested. Several wide-angle frames have remarkably similar cumulative crater size frequency distributions that may be representative of a large portion of the martian surface.*

The general characteristics of the martian surface, the size frequency distribution of craters visible on some Mariner 6 and Mariner 7 frames, and various crater shapes have been reported (*1*). The distribution and crater characteristics of light and dark areas of the martian surface also have been studied (*2*). However, earlier studies revealed neither obvious correlations of crater abundances with the albedo of the surface, nor differences in crater morphologies across the contacts between light and dark areas in different localities.

We selected three Mariner 6 near-encounter images (6N11, 6N13, and 6N19) having approximately the same resolution and drew the approximate contact between light and dark (higher and lower albedo) terrains, using both the photometrically corrected and the maximum-discriminability imagery (Figs. 1 and 2). The area investigated lies within 5°N to 22°S latitude and 348° to 13°W longitude (*3*). The craters on these two different albedo surfaces were identified and measured (181 craters in dark terrain, 147 craters in light terrain), and the crater diameters were corrected for spacecraft viewing angle. Craters smaller than 5 km were not counted because of the difficulty of recognition and accurate measurement at the resolution of the images. The exact position of the light-dark contact has little influence on the cumulative size frequency distributions because only a small percentage of the craters are within the area of uncertainty of the contact. The craters identified are not entirely coincident with those measured by Cutts *et al.* (*2*) on the same frames, probably because of unavoidable subjectivity in the recognition of indistinct craters (*4*). The cumulative crater size frequency distributions were plotted with probability ordinates (Figs. 3 and 4) so that random samples from like populations or the same population would graph identically, provided that the sample size is sufficient. Differences between curves are solely a function of differences in the size distribution within the populations, and cratering density differences are nowhere displayed on these curves [for further discussion see (*5*)]. The cumulative size frequency distributions of craters on frames 6N11, 6N13, and 6N19 (Fig. 4) appear to be part of the same population. However, if the cumulative size frequency distributions of craters on the light and dark terrains of the mosaic are plotted separately (Fig. 3), a large displacement (*6*) of the two curves occurs between the 20-km and 50-km crater diameters, and possibly extends to even larger crater diameters. The divergence of the cumulative size frequency distribution curves is caused by a greater proportion of larger craters in the light terrain as compared to the dark terrain. More-

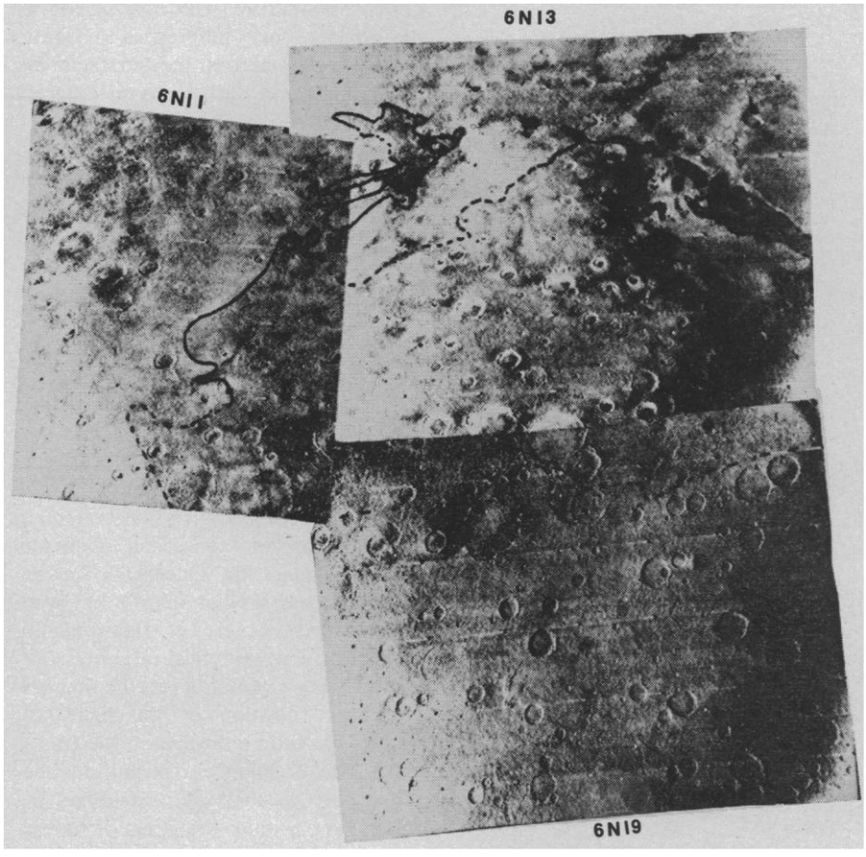

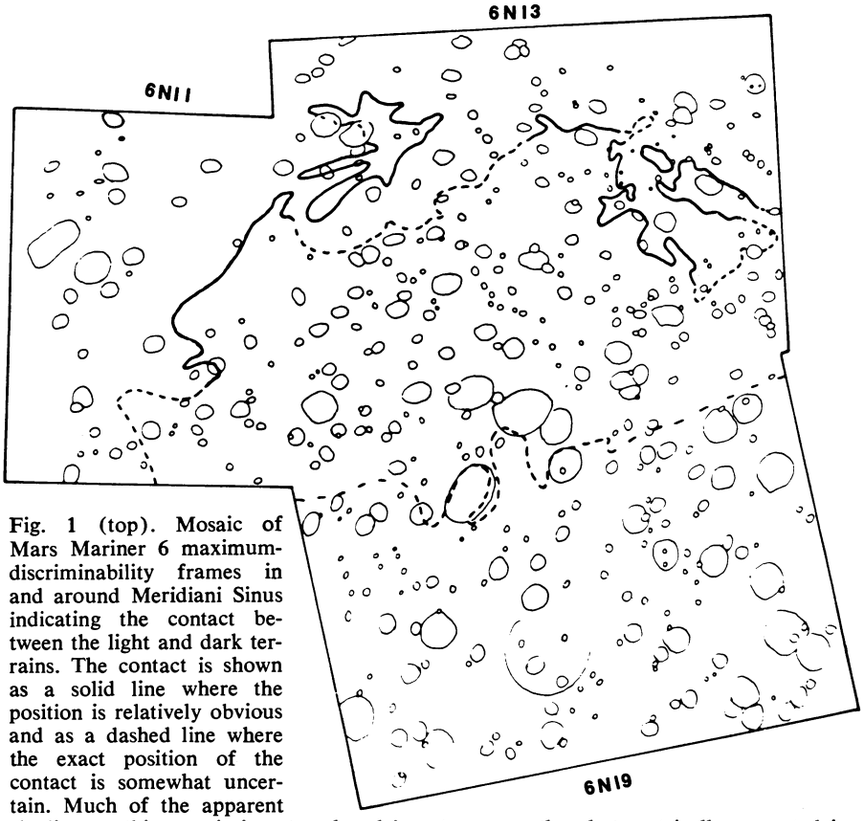

Fig. 1 (top). Mosaic of Mars Mariner 6 maximum-discriminability frames in and around Meridiani Sinus indicating the contact between the light and dark terrains. The contact is shown as a solid line where the position is relatively obvious and as a dashed line where the exact position of the contact is somewhat uncertain. Much of the apparent shading on this mosaic is not real and is not seen on the photometrically corrected imagery. Fig. 2 (bottom). Outline of the mosaic of Mariner 6 frames in and around Meridiani Sinus showing the approximate position of the contact between the light and dark terrains and the approximate locations of the craters that were measured and counted.

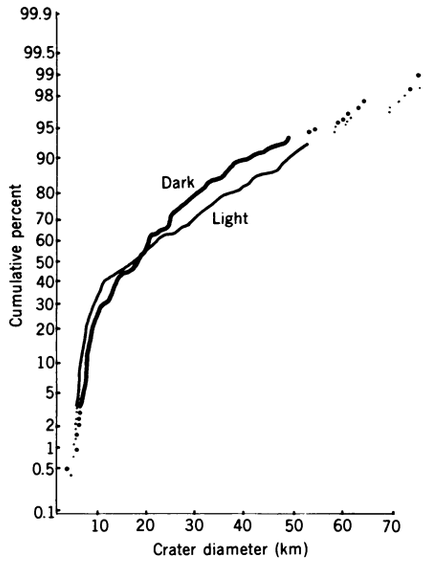

Fig. 3. Cumulative crater size frequency distributions on the light and dark terrains in and around Meridiani Sinus (frames 6N11, 6N13, 6N19). This plot shows that the population of craters on the light terrain contains a greater proportion of craters in the diameter range from 20 to 50 km. It is also apparent that the crater population of the light terrain is impoverished in small craters (this graph nowhere displays crater densities per unit area).

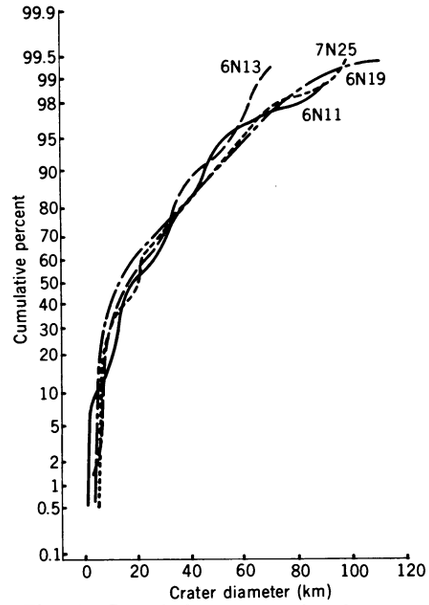

Fig. 4. Cumulative crater size frequency distributions on four wide-angle frames from Mariner 6 and Mariner 7. These curves are markedly similar and probably are part of the same population. The general shape and position of this curve may approximate the distribution for a large portion of the martian surface at the resolution of the Mariner 6 and Mariner 7 images.

over, the dark terrain has an excess of craters smaller than 15 km in diameter as compared to the light terrain. In addition, the dark terrain has a higher total number of craters per unit area (Fig. 2); the ratio of the total crater density on the dark terrain to that on the light terrain is approximately 7:5.

The best interpretation for the fact that there is a higher density of larger craters on the light terrain as compared to the dark terrain probably is that the light terrain has a greater impact exposure age. The greater total number of craters per unit area on the dark terrain probably is a function of either more rapid erosion and filling of craters (particularly the smaller sizes) on the light terrain or greater production of small endogenetic craters in the dark terrain, or both. Polarimetric and photometric data for Mars were found to be consistent with mean particle sizes of 100 to 200 μm on the dark areas and 25 μm on the light areas, and the finer-sized material on the light terrain would be more easily transported by the surface and atmospheric processes hypothesized for Mars (*7*). It seems possible that the finer-sized particles might be more available to fill and erode the craters on the light terrain than would the coarser surface particles on the dark terrain. We propose that the lighter terrain is generally older than the dark terrain (frames 6N11, 6N13, and 6N19), but that the surface of the older light terrain may be covered with relatively young, mobile detritus.

The crater size frequency distributions of four wide-angle frames (6N11, 6N13, 6N19, and 7N25) coincide very closely (Fig. 4). These frames include a large total area and both light and dark terrains, and the average of these curves may approximate the size frequency distribution of craters of a large portion of the martian surface.

ALEXANDER WORONOW
ELBERT A. KING, JR.
Department of Geology, University of Houston, Houston, Texas 77004

References and Notes

1. B. C. Murray, L. A. Soderblom, R. P. Sharp, J. A. Cutts, *J. Geophys. Res.* **76**, 313 (1971).
2. J. A. Cutts, L. A. Soderblom, R. P. Sharp, B. A. Smith, B. C. Murray, *ibid.*, p. 343.
3. M. E. Davies and R. A. Berg, *ibid.*, p. 373.
4. A. B. Binder, *Science* **164**, 297 (1969).
5. S. S. Wilks, *Elementary Statistical Analysis* (Princeton Univ. Press, Princeton, N.J. 1948); T. H. Brown, R. F. Bingham, V. A. Temnomeroff, *Laboratory Handbook of Statistical Methods* (McGraw-Hill, New York, 1931).
6. The mean diameters of the craters are as follows: light terrain, 27 km; dark terrain, 23 km. The standard deviation is 17 km for the light terrain and 11 km for the dark terrain. Maximum displacement between the two curves is approximately 11 km or 1 standard deviation at 85 cumulative percent. However, we should not expect differences of 2 or 3 standard deviations if the difference in age of the two surfaces is relatively small. Furthermore, there is an underlying assumption that the size and velocity frequency distribution of meteoroids near Mars did not change drastically during the interval between the age of the two surfaces.
7. J. B. Pollack and C. Sagan, *Space Sci. Rev.* **9**, 243 (1969).
8. This work was supported by the National Aeronautics and Space Administration.

1 June 1971; revised 26 October 1971

Cyclic Nucleotide Phosphodiesterase: High Activity in a Mammalian Photoreceptor

Abstract. *Purified outer segments of bovine rods exhibit phosphodiesterase activity against adenosine and guanosine cyclic 3',5'-monophosphates (cyclic AMP and cyclic GMP). The enzyme hydrolyzed cyclic GMP more rapidly than cyclic AMP at low substrate concentrations. The presence of high phosphodiesterase activity in this highly specialized organelle suggests that this enzyme may function in control of cyclic nucleotide concentration during visual excitation or adaptation.*

The process by which the retina translates light energy into a nerve impulse is only partially understood. Much has been learned about both the bleaching of rhodopsin (*1*) and the ensuing electrophysiological changes which occur in the retina (*2*), but the mechanism linking these phenomena remains unknown. There would seem to be two criteria that this translating mechanism must fulfill. (i) It must achieve significant amplification, since bleaching of one rhodopsin molecule is sufficient to excite a receptor cell. (ii) This process must act over a distance, since in rods and primate cones the lamellae containing the rhodopsin are separated from the plasma membrane (*3*). Wald has proposed that the bleaching of rhodopsin might alter the activity of an enzyme (*4*). This suggestion has been given added impetus by the observation of Bitensky *et al.* (*5*) that outer segments of frog rods contain a light-inhibited adenylate cyclase. For this inhibition to significantly affect concentration of cyclic nucleotides within the short time in which visual excitation occurs, the receptor region of the retina must also contain high activity of phosphodiesterase, the enzyme which destroys cyclic AMP (*6*). As shown in Table 1, we have found this to be the case in outer segments of bovine rods.

Cattle eyes were obtained from a local slaughterhouse and dark-adapted in the cold overnight. Subsequent operations were carried out in dim light. The retinas were dissected out and swirled in 0.25*M* sucrose that contained 5 m*M* $MgCl_2$ and 10 m*M* tris(hydroxymethyl)-aminomethane (tris), *p*H 8.1. The suspension was filtered through a double layer of cheesecloth, and crude rod outer segments were obtained from the filtrate by centrifugation over a 41 percent sucrose cushion at 5000 rev/min in a Spinco SW-27 rotor (3200*g*) for 1 hour. This preparation was then centrifuged on a continuous sucrose density gradient (24 to 41 percent) for 12 hours at 25,000 rev/min (83,000*g*). A band containing pure rod outer segments, as determined by light and electron micros-

Table 1. Cyclic AMP phosphodiesterase. Enzyme activity is expressed as nanomoles of cyclic AMP hydrolyzed per minute per milligram protein. Samples of brain and retina from adult rats and 16-day chick embryos were homogenized in a solution containing 2 m*M* glycylglycine, 10 m*M* NaCl, and 10 m*M* KCl, *p*H 7.4. Rod outer segments were prepared as described in the text. Enzyme activity, measured as oxidation of reduced nicotinamide adenine dinucleotide (NADH), was monitored continuously by absorbance at 340 nm. The reaction mixture contained 0.1*M* tris buffer at *p*H 7.5, 5.5 m*M* α-ketoglutaric acid, 0.1 m*M* ethylenediaminetetraacetic acid, 0.1 m*M* NADH, 0.25 m*M* nicotinamide adenine dinucleotide, 1 m*M* $MgCl_2$, 2 m*M* cyclic AMP, *Escherichia coli* alkaline phosphatase (25 μg/ml), adenosine deaminase (0.02 μg/ml), and glutamic acid dehydrogenase (0.25 mg/ml) (*12*). Samples were assayed in duplicate under conditions in which reaction rate was a linear function of protein concentration. These values were corrected for the rate in the absence of cyclic AMP (which was negligible in the samples of rod outer segments). Protein was measured by the method of Lowry *et al.* (*13*).

Source	Enzyme activity
Rat brain	39
Rat retina	8.4
Chick brain	44
Chick retina	42
Bovine retina	15
Bovine rod outer segment	82